High accuracy measurement of Poisson's ratio of optical fibers and its temperature dependence using forward-stimulated Brillouin scattering

L. A. Sánchez,[1] **A. Díez,[1,2,*]** **J. L. Cruz,[1,2]** AND **M. V. Andrés[1,2]**

[1]*Laboratory of Fiber Optics, ICMUV, Universidad de Valencia, Dr. Moliner 50, 46100 Burjassot, Spain*
[2]*Departamento de Física Aplicada y Electromagnetismo, Universidad de Valencia, Dr. Moliner 50, 46100 Burjassot, Spain*
*antonio.diez@uv.es

Abstract: Transverse acoustic mode resonances enable a high accuracy determination of Poisson's ratio and elastic properties of optical fibers. An all-optical pump and probe technique is used for efficient excitation and accurate characterization of both, radial and torsional-radial acoustic resonances of optical fibers. Simple and precise algebraic expressions for the frequencies of high order acoustic resonances are derived, enabling a rigorous analysis of the experimental data using standard least squares fitting. Following this approach, the determination of Poisson's ratio does not require the measurement of any physical length, but only frequency measurements are required. An accuracy better than 1 ‰ is achieved. The dependence of the fiber Poisson's ratio with temperature is also determined experimentally.

1. Introduction

Optical fiber technology based on silica glass is a well stablished technology. However, an accurate determination of Poisson's ratio (ν) is still required. It is somewhat surprising the limited knowledge that is available on optical fiber Poisson's ratio. Most reported values were measured for bulk silica, but a significant difference is usually observed with the experimental values obtained for silica optical fibers. A value ranging between 0.16 and 0.17 is assumed, with an uncertainty of ± 0.01, i.e., a relative error of 6%. Two lines of research can benefit from an accurate knowledge of Poisson's ratio and its dependence with temperature ($\mathrm{d}\nu/\mathrm{d}T$): the study of photoelastic effects in optical fibers (i.e., the determination of Pockels coefficients), and the development of fiber sensors.

Earlier studies of photoelastic effects in optical fibers assumed a value of either 0.16 or 0.17 for Poisson's ratio of fused silica [1,2], and this has not changed with time. The uncertainty of the Poisson's ratio is the dominant factor limiting the precision with which Pockels coefficients were determined in the past [3], where relative errors of around 10% were common. Any attempt to measure the chromatic dispersion of Pockels coefficients of silica [4] is limited by the uncertainty of ν [3,5]. The development of fiber sensors requires as well an accurate determination of Poisson's ratio. The design and optimization of strain sensors based on fiber Bragg gratings (FBGs) requires accurate knowledge of the Poisson's ratio and its temperature dependence. For instance, in [6] the authors are compelled to use values obtained for bulk silica with 10% error [7] for modeling the response of regenerated FBG.

Sensor applications of fiber interferometers usually require to model coated fibers with a multilayer that combine adhesives, polymer coatings, and specific sensor materials (for example, terfenol-D for magnetic field sensors) [8–10]. These works on magnetic field sensors, geophysical applications and fiber optic gyroscopes assume a constant value for ν, although they identify the

importance of temperature effects, so all of them will benefit from an accurate determination of ν, and $d\nu/dT$.

The classical approaches to determine ν and $d\nu/dT$ in bulk samples of fused silica are based on measuring both longitudinal and shear velocities. This is achieved either measuring the lower flexural and torsional frequencies of resonance [7] or using an ultrasonic pulse method with time detection [11]. Photoelastic effects can be used to evaluate ν, both using bulk samples [4] and optical fibers [3,12], although it gives relatively high uncertainty of about 10% or even higher. The techniques based on the photoelastic effects combine typically some interferometric and polarimetric measurements.

Here, we report a new technique based on all-optical excitation and detection of transverse acoustic mode resonances (TAMRs) in the optical fiber. After measuring the frequencies of a relatively large number of TAMRs, the normalized longitudinal and shear velocities is determined, and Poisson's ratio is derived without requiring any measurement of fiber dimensions. In addition, this technique benefits from the high Q values of the acoustic resonances, which enables the determination of resonance frequencies with low uncertainty. In parallel, the derivation of precise asymptotic expressions for the different families of acoustic resonances gives simple analytical expressions that fit accurately the experimental measurements.

The interaction between light and sound in a medium is a fundamental phenomenon in physics that researchers have investigated for many decades. Light waves can stimulate mechanical vibrations through electrostriction and/or radiation pressure, while acoustic waves can scatter and modulate light through the elasto-optic effect. A fundamental interaction between light and acoustic waves is Brillouin scattering. Backward stimulated Brillouin scattering (BSBS) is induced by longitudinal acoustic waves and has important implications in many different fields, as for example, in ultra-narrow bandwidth lasers [13,14], slow- and fast-light [15,16], microwave signal processing [17,18], and optical signal storage [19,20]. Among all the exciting applications of BSBS, optical fiber sensing is of remarkable relevance: BSBS enables high-resolution distributed sensing [21], strain and temperature with sub-meter scale resolution along tens of km of the optical fiber can be performed [22].

Forward stimulated Brillouin scattering (FSBS) is an opto-acoustic effect that occurs when light is scattered by TAMRs of the optical fiber, which are excited through electrostriction by an optical pump wave. The properties of TAMRs, and therefore of FSBS, are dependent on the fiber properties. That includes temperature and strain, thus, FSBS-based sensing techniques for strain [23], and temperature [24,25] have been demonstrated in the past. Sound velocity measurement in optical fibers was also performed, including a low accuracy measurement of Poisson's ratio [26].

Recently, there has been an increasing interest on the development of innovative sensing applications based on FSBS. Unlike sensors based on backward BSBS, which are restricted to detect physical parameters inside the fiber core, FSBS is also dependent on the fiber surroundings, therefore, new sensing opportunities, not affordable for BSBS sensors can be addressed using FSBS. For instance, sensing of liquids surrounding an optical fiber has been demonstrated through the measurement of the liquid acoustic impedance [27,28]. On the other hand, recent demonstration of various schemes that enable distributed fiber sensing based on FSBS [29–31] has boosted the interest of FSBS as physical mechanism for fiber sensing.

The TAMRs behind FSBS in standard optical fibers are generated by radial modes $R_{0,m}$ and torsional-radial modes $TR_{2,m}$ [32]. Both are excited by electrostriction when an optical pulse propagates in the fiber. Most of the applications based on TAMRs and FSBS, reported so far, exploit the properties of either $R_{0,m}$ radial acoustic resonances or torsional-radial $TR_{2,m}$ acoustic resonances. Here we show that the potentiality of TAMRs for fiber sensing/metrology can be extended further by taking into account, and combining the characteristics and response of both

type of resonances. We apply this concept for the measurement of Poisson's ratio with high accuracy.

2. Theory

In standard optical fibers, the mechanical properties of core and cladding materials are very similar. Additionally, the core diameter of a single mode fiber is much smaller than the cladding, thus, the core has little impact on the properties of low frequency acoustic modes. Therefore, from the mechanical point of view, a standard optical fiber is commonly considered as an isotropic cylinder made of silica. The study of vibrational modes in a uniform cylinder shows that the acoustic modes depend on the cylinder radius a, and the longitudinal and shear acoustic velocities V_L and V_S, which determine the wave number along the axis of the cylinder q at a given frequency. Transverse acoustic resonances $R_{0,m}$ and $TR_{2,m}$ correspond to a particular case in which $q = 0$. The first, $R_{0,m}$ modes are dilatational modes; their displacement field contains only the radial component, and depends only on the radial coordinate [33]. The strain field created by $R_{0,m}$ modes is radially symmetric, and it produces pure phase modulation of the light propagating in the fiber core. The displacement vector of $TR_{2,m}$ modes includes the radial and the angular component, depending both on the radial and angular coordinates [33]. They induce birefringence in the fiber due to the angular variation of the transverse displacement, which affects the polarization of the light. The characteristic equations for $R_{0,m}$ and $TR_{2,m}$ resonances are, respectively, given by [34]:

$$(1 - \alpha^2) J_0(\alpha z) - \alpha^2 J_2(\alpha z) = 0 \quad (R_{0,m} \text{modes}) \tag{1}$$

$$\begin{vmatrix} \left(3 - \frac{z^2}{2}\right) J_2(\alpha z) & \left(6 - \frac{z^2}{2}\right) J_2(z) - 3 z J_3(z) \\ J_2(\alpha z) - \alpha z J_3(\alpha z) & \left(2 - \frac{z^2}{2}\right) J_2(z) + z J_3(z) \end{vmatrix} = 0 \quad (TR_{2,m} \text{modes}) \tag{2}$$

where z is the normalized frequency given by $z = 2\pi a f / V_S$, and $\alpha = V_S / V_L$, being f the resonance frequency. Notice that the characteristic equation for $TR_{2,m}$ modes is expressed in the form of a determinant of a 2×2 matrix equal to zero. Solving the above characteristic equations, the theoretical frequencies of resonance of $R_{0,m}$ and $TR_{2,m}$ modes can be computed.

In what follows, we derive accurate asymptotic expressions for the characteristics equations that give an interesting physical insight, and enable simple fitting of the experimental data to analytical expressions. We use Hankel's asymptotic expansions of Bessel functions for large arguments (see Eq. 9.2.1 in Ref. [35]). Once common factors in Eq. (1) are cancelled out, we will retain the terms proportional to z^0, and z^{-1}. Thus, the characteristic equation of $R_{0,m}$ modes can be approximated by the expression:

$$\cot(\alpha z - \pi/4) = \frac{16 \alpha^2 - 1}{8 \alpha z} \tag{3}$$

This result can be further reduced by taking into account that the right-hand side is nearly zero for large values of z. Thus, using the Taylor expansion of the cotangent at the zeroes of the function given by $\alpha \cdot z_m - \pi/4 = m \cdot \pi - \pi/2$, $m = 1, 2, 3, \ldots$ and evaluating the right-hand side of Eq. (3) at $z = z_m$, we obtain our final asymptotic expression for the characteristic equation of $R_{0,m}$ acoustic resonances:

$$\alpha z_{R,m} = c_m - \frac{16 \alpha^2 - 1}{8 c_m}, \text{ being } c_m = m\pi - \pi/4, \ m = 1, 2, 3, \ldots \tag{4}$$

In order to analyze the $TR_{2,m}$ resonances, we first rewrite Eq. (2) in the form:

$$J_2(z) J_2(\alpha z) = \Delta \tag{5}$$

$$\Delta = \frac{[(6 - z^2/2)J_2(z) - 3\,z\,J_3(z)][J_2(\alpha\,z) - \alpha\,z\,J_3(\alpha\,z)]}{(3 - z^2/2)(2 - z^2/2)} \tag{6}$$

Using again the Hankel asymptotic expansions of Bessel functions for large arguments, we find that the right-hand side of Eq. (5) is small (in fact, we will see later that the dominant term is proportional to $1/z^2$). Being $\Delta \approx 0$, Eq. (5) permits to identify two series of $TR_{2,m}$ modes, whose frequencies are determined by the solutions $J_2(z) \approx 0$ and $J_2(\alpha\,z) \approx 0$, respectively, assuming non degenerated resonances. Following the same steps that have been described when deriving Eqs. (3) and (4), we find for the first series, denoted as $TR_{2,m}^{(1)}$, that the normalized frequencies, $z_{TR,m}^{(1)}$, can be approximated by the solutions of equation:

$$\cot(z - 5\pi/4) = \frac{15}{8\,z} + \frac{\Delta}{\sin(z - 5\pi/4)J_2(\alpha\,z)} \tag{7}$$

Now, taking into account that the right-hand side is nearly zero for large values of z, we will use the Taylor expansion of the cotangent at the zeroes of the function given by $z_m - 5 \cdot \pi/4 = m \cdot \pi - \pi/2$, m = 1, 2, 3, ... When the right hand side of Eq. (7) is evaluated at $z = z_m$, we find that the dominant term in Δ is proportional to $1/z_m^2$, provided $J_2(\alpha\,z) \neq 0$, i.e., the resonances of the first series are not degenerated with the resonances of the second series. Thus, neglecting Δ, we find that the normalized frequencies of the first series of torsional radial modes, $TR_{2,m}^{(1)}$, can be approximated by:

$$z_{TR,m}^{(1)} = c_{m+1} - \frac{15}{8\,c_{m+1}} \tag{8}$$

where c_m was defined in Eq. (4). Similarly, the normalized frequencies of the second series of torsional radial modes, $TR_{2,m}^{(2)}$, can be approximated by:

$$z_{TR,m}^{(2)} = (1/\alpha)z_{TR,m}^{(1)} \tag{9}$$

These results show up an interesting property. The $TR_{2,m}$ acoustic modes are composed of two series. The asymptotic values of the normalized frequencies of one series depend mainly on the
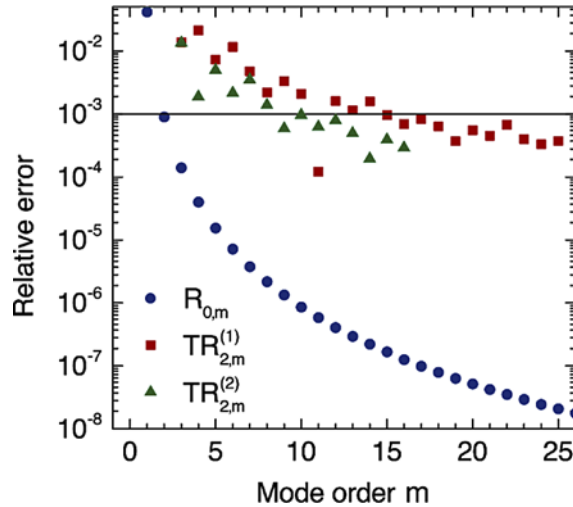

Fig. 1. Relative difference between exact and approximated frequencies of $R_{0,m}$, $TR_{2,m}^{(1)}$ and $TR_{2,m}^{(2)}$ resonances for $\alpha = 0.63$.

velocity V_S, while for the second series depend on V_L, as in the case of the asymptotic values of resonances $R_{0,m}$ (see Eq. (4)).

In order to estimate the difference between the values derived from the asymptotic expressions, (4), (8) and (9), and the exact solutions, (1) and (2), we have evaluated the relative error taking $\alpha = 0.63$ (close to the expected value for a silica optical fiber). Figure 1 shows the relative difference for the radial and torsional-radial resonances. In all cases, the relative difference decreases with the mode order m. If we take as a reference a value of one thousandth, we find that, for $R_{0,m}$ resonances, the asymptotic expression gives a relative error lower than 10^{-3} from $m = 2$, while for $TR_{2,m}^{(1)}$ and $TR_{2,m}^{(2)}$ resonances it is from $m = 15$ and $m = 10$, respectively. Therefore, we can conclude that the above asymptotic expressions can be used to evaluate the resonant frequencies of $R_{0,m}$ and $TR_{2,m}^{(1,2)}$ resonances with an error below one thousandth for high order resonances (in particular, $m \geq 2$ for $R_{0,m}$, and $m \geq 15$ for $TR_{2,m}^{(1)}$).

3. Experimental results

3.1. Experimental setup

An LPG-assisted pump-and-probe method was used to investigate TAMRs in a standard single-mode optical fiber [36]. Transverse acoustic resonance modes were excited in the optical fiber through electrostriction by an optical pump pulse propagating along it. The acoustic resonances generated in the fiber were detected by means of a narrow-band long-period fiber grating (LPG) that was inscribed in the core of the fiber under test. The LPG is modulated by the excited acoustic waves through the photo-elastic effect. The response of the LPG is sensed by a probe laser tuned to one edge of the LPG notch. In this technique, the sensing element, i.e. the LPG is just few cm in length. This contributes to reduce remarkably the linewidth of the measured acoustic resonances, and helps to improve the accuracy of the results obtained in the present work. More details about the excitation and detection of the resonances can be found in [36].

The schematic diagram of the experimental setup is shown in Fig. 2(a). A Q-switched microchip laser (TEEM Photonics SNP-20F-100) emitting at 1064 nm was used as the pump to generate the acoustic wave inside the fiber. This laser emits pulses of 700 ps duration with a period of 52.6 µs. A half-wave plate was placed at the output of the pump laser to adjust the polarization and optimize the excitation of torsional-radial modes. A counter-propagating 1.5 µm continuous-wave tunable laser (Keysight 81940 A) was used to interrogate the transmission of the LPG. A polarization controller (PC) was used to adjust the polarization state of the probe laser to one of the principal axes of the optical fiber (since the LPG has a narrow linewidth of about 1 nm, the residual birefringence of a standard fiber produces the splitting of the LPG transmission spectrum [37]). Finally, the response of the grating was interrogated using a fast photodetector (Newport 1611FC-AC) and an oscilloscope (Keysight DSOS104A).

The optical fiber used in the experiments was a piece of single-mode fiber SM1500 (4.2/125) from Fibercore. A narrow-band LPG was written in the fiber following the method described in [37]. The spectrum of the grating is shown in Fig. 2(b). The period of the LPG was 52.3 µm, the length was 11 cm. The LPG notch was centered at 1551 nm and its bandwidth was 1.3 nm. A fiber section of SMF980 was spliced at the input of the LPG to optimize the coupling of the pump pulses to the fundamental mode of fiber SM1500.

Measurements as a function of temperature were performed by placing the fiber SM1500 with the LPG in a cooling-heating temperature chamber (WTB Binder MK 53), covering in our experiments a temperature range from $-20°$ to 80 °C. Temperature inside the chamber was measured using a temperature meter (Di-LOG DL7102) with a temperature accuracy of 0.8 °C.
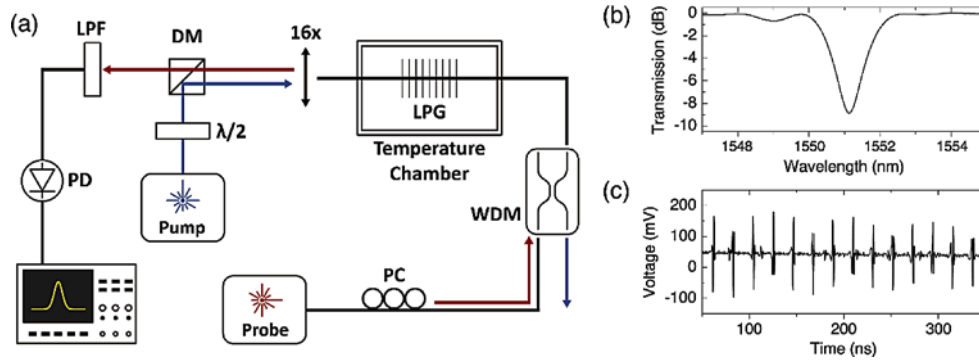
Fig. 2. (a) Experimental setup. PD: photodetector; LPF: long-pass filter; DM: dichroic mirror; WDM: wavelength division multiplexer. (b) LPG spectrum, (c) temporal response of the probe beam transmitted by the grating.

3.2. Results

The acoustic waves excited by the pump pulse generates an oscillatory response in the transmission of the LPG that produces a sequence of intensity oscillations in the probe beam, with amplitude decaying with time. Figure 2(c) shows an example. The radio-frequency (RF) spectrum of the probe signal contains a series of peaks corresponding to the different $R_{0,m}$ and $TR_{2,m}$ mode resonances excited. Figure 3 shows the spectrum of the TAMRs between 150 MHz and 500 MHz at 20 °C. The different peaks are labelled according to the mode series to which they belong. As expected from the theoretical analysis, at high frequencies the resonances for the $TR_{2,m}^{(2)}$ modes are very close to that of the $R_{0,m}$ modes, which makes them difficult to be observed. However, the high Q values of the acoustic resonances that results from the method employed permits to identify the $TR_{2,m}^{(2)}$ resonances up 800 MHz.
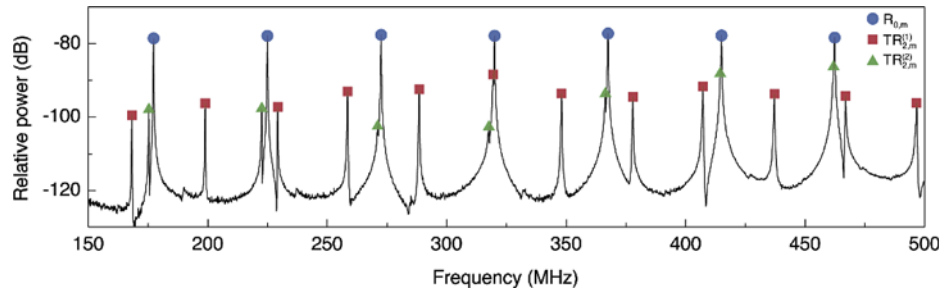

Fig. 3. TAMRs spectrum from 150 MHz to 500 MHz. $R_{0,m}$ modes are denoted by circles while $TR_{2,m}^{(1)}$ and $TR_{2,m}^{(2)}$ are denoted by squares and triangles, respectively.

TAMRs were characterized in detail as a function of temperature. Peaks corresponding to $R_{0,m}$ modes from $m = 5$ to $m = 23$ and $TR_{2,m}^{(1)}$ modes from $m = 12$ to $m = 28$ were recorded in a range of temperatures of $[-20, 80]$ °C in steps of 5 °C. As an example, Fig. 4(a) shows the frequency displacement of the $R_{0,8}$ and the $TR_{2,18}^{(1)}$ resonances for different temperatures. Resonance frequency values were obtained after computing the Fourier transform of the temporal response of the LPG with an error lower than 30 kHz (a direct measurement with an RF spectrum analyzer was also performed, with the same results).

The relative frequency shift $\Delta f/f$ of all modes belonging to a given series –either the $R_{0,m}$ or the $TR_{2,m}^{(1)}$ resonances– was the same within the experimental error. Figure 4(b) shows $\Delta f/f$
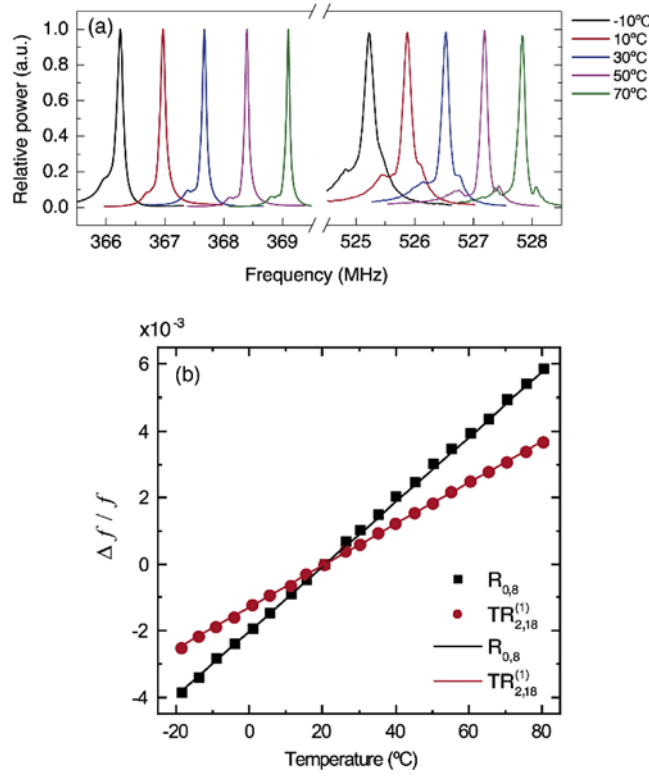
Fig. 4. (a) RF spectrum for different temperatures corresponding to $R_{0,8}$ (left) and $TR_{2,18}^{(1)}$ (right) modes. (b) Relative frequency shift for $R_{0,8}$ and $TR_{2,18}^{(1)}$ modes. The dots correspond to the experimental data and the lines to their linear fit.

as a function of temperature for the $R_{0,8}$ and $TR_{2,18}^{(1)}$ resonances, along with a linear fitting. The resonances shift linearly with temperature, with $\Delta f / f$ shift rate of $(9.76 \pm 0.06) \times 10^{-5}$ °C^{-1} for $R_{0,m}$ modes and $(6.25 \pm 0.04) \times 10^{-5}$ °C^{-1} for $TR_{2,m}^{(1)}$ modes.

3.3. Discussion

Following the analysis developed in section 2, at each temperature the experimental resonance frequencies of the $R_{0,m}$ and $TR_{2,m}^{(1)}$ modes were, respectively, fitted to the following functions,

$$f_{R,m} = A \ (c_m - B/c_m) \tag{10}$$

$$f_{TR,m}^{(1)} = C \ [c_{m+1} - 15/(8 \cdot c_{m+1})] \tag{11}$$

were A, B, and C are fitting parameters. Figure 5 shows the experimental resonance frequencies for both series of modes recorded at room temperature, along with the least squares fits. Missing points in the $TR_{2,m}^{(1)}$ series correspond to resonances that were not observed since their values are very close to that of a $R_{0,m}$ resonances, so their peaks in the RF spectrum were overlapped.

As seen from the expression for the normalized frequencies, Eqs. (4) and (8), fitting parameters A and C are $V_L/(2\pi a)$ and $V_S/(2\pi a)$, respectively. For example, at room temperature the values obtained are $V_L/a = (94.463 \pm 6 \times 10^{-3})$ m·s^{-1} μm^{-1} and $V_S/a = (59.345 \pm 9 \times 10^{-3})$ m·s^{-1} μm^{-1}. The acoustic velocities could be obtained provided the fiber radius is measured. Given the errors of V_L/a and V_S/a, the precision with which V_L and V_S can be obtained is essentially determined
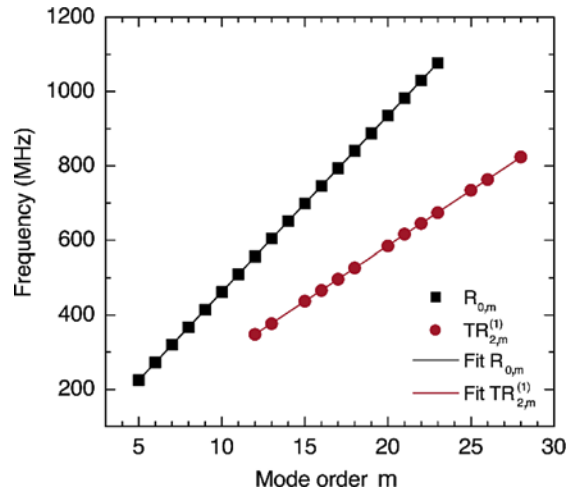
Fig. 5. Experimental resonance frequencies for $R_{0,m}$ and $TR_{2,m}^{(1)}$ modes recorded at 20°C, along with their fits.

by the precision of the fiber radius measurement, at least for radius uncertainties higher than 1 nm.

The Poisson ratio of the optical fiber can be obtained from the experimental analysis, without requiring the measurement of the fiber radius. The Poisson ratio, ν, of a given material can be expressed as a function of the ratio between the acoustic velocities α [38],

$$\nu = \frac{1 - 2\,\alpha^2}{2(1 - \alpha^2)} \tag{12}$$

Then, the Poisson ratio of the optical fiber can be obtained from the fits of the asymptotic expressions to the experimental data, by dividing the slopes C and A. Since the measurement of the fiber radius is not required, thus, the accuracy of ν is not determined by the radius uncertainty. Note that the development of algebraic expressions to describe the resonance frequencies allows a simple and precise fit of all the experimental data of a given mode series at once, which certainly contributes to reduce the error of the parameters that result from this analysis. We estimate that the absolute error with which Poisson's ratio is obtained is $\pm\,2 \times 10^{-4}$. To our knowledge, this is about two orders of magnitude smaller than usually reported values, and at least one order of magnitude smaller than the value reported in Ref. [11] (see in Table 1 a comparison of ν values at room temperature).

Taking advantage of the high accuracy provided by the method described above, we investigated the variation of the optical fiber Poisson's ratio with temperature. The procedure described above was repeated for the spectra recorded at different temperatures. Figure 6 shows V_L/a and V_S/a obtained experimentally, and the resulting Poisson's ratio, as a function of temperature. Within the temperature range of our experiments, the dependence of Poisson ratio on temperature is linear The line of best fit was calculated using the procedure reported in [39],

$$\nu = (0.17316 \ \pm \ 2 \times 10^{-5}) \ + \ T \cdot \ [(3.76 \ \pm \ 0.04) \times 10^{-5}] \ (^{\circ}\,\mathrm{C}^{-1}) \tag{13}$$

Notice that, since the procedure that provides the Poisson's ratio does not depend of the fiber radius, fiber thermal expansion is not an issue that needs to be taken into consideration. Table 1 provides a comparison of the temperature coefficient of ν with values that can be found in the literature for bulk samples of fused quartz (no value has been reported for an optical fiber, as far as the authors know).

Table 1. Poisson's ratio and its temperature variation

Sample	ν (at 20 °C)	$d\nu/dT$ (10^{-5}/K)	Ref. / Measuring technique
Optical fiber SM1500	0.1740 ± 0.0002	3.76 ± 0.04	Present work / FSBS-resonances (TAMRs): measuring $R_{0,m}$ and $TR_{2,m}^{(1)}$
Optical fiber	0.17 ± 0.02	- - -	[12] / Interferometric measurement of photoelastic effects
Optical fiber	0.154 ± 0.018^a	- - -	[3] / Interferometric and polarization measurements of photoelastic effects
Bulk sample	0.1727 ± 0.0015^a	9.6 ± 0.2^a	[11] / Ultrasonic pulse method
Optical fiber	0.17^a	- - -	[26] / FSBS-resonances: measuring TR_{25} and TR_{27}
Bulk sample	0.164^a	- - -	[4] / Interferometric measure-ment of Photoelastic effects
Bulk sample	0.165 ± 0.017^a	4.0	[7] / Measurement of flexural and torsional resonances

[a]Values derived from Fig. 3 in Ref. [11] in the temperature range $[-20, 80]$ °C
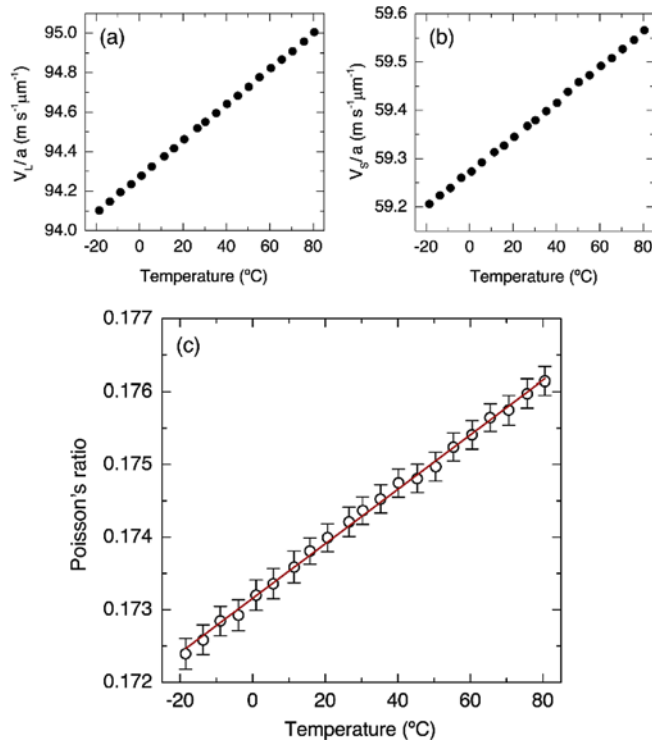[b]Measurements at room temperature

Fig. 6. Experimental ratios (a) V_L/a and (b) V_S/a versus temperature. (c) Poisson's ratio, as a function of the temperature of the optical fiber used in the experiment.

4. Conclusion

A technique based on transverse acoustic mode resonances has been reported for accurate measurement of Poisson's ratio in optical fibers. The precision of the technique relies on two features: (1) the result is derived from frequency measurements, and (2) no length measurement is required. The technique takes into account the whole experimental information provided by

both series of radial and torsional-radial acoustic resonances, and benefits from the derivation of algebraic asymptotic expressions to calculate the resonance frequencies of both types of resonances, which allows performing accurate fittings of the experimental data. The method has been applied to silica optical fibers and the Poisson's ratio was obtained with an estimated relative error lower than 1 ‰. The high precision of the present technique allowed us investigating the dependence of the fiber Poisson's ratio with temperature. It is found that it increases linearly with temperature at a rate of 3.76×10^{-5} °C^{-1}. The method has been applied to silica optical fibers, although it can eventually be applied to fibers based on other materials. Moreover, the method can be extended to measure other elastic properties of optical fibers.

Disclosures. The authors declare no conflicts of interest.

Data availability. Data underlying the results presented in this paper are not publicly available at this time but may be obtained from the authors upon reasonable request.

References

1. A. M. Smith, "Birefringence induced by bends and twists in single-mode optical fiber," Appl. Opt. **19**(15), 2606 (1980).
2. R. Ulrich, S. C. Rashleigh, and W. Eickhoff, "Bending-induced birefringence in single-mode fibers," Opt. Lett. **5**(6), 273 (1980).
3. A. Bertholds and R. Dandliker, "Determination of the individual strain-optic coefficients in single-mode optical fibres," J. Lightwave Technol. **6**(1), 17–20 (1988).
4. W. Primak and D. Post, "Photoelastic Constants of Vitreous Silica and Its Elastic Coefficient of Refractive Index," J. Appl. Phys. **30**(5), 779–788 (1959).
5. X. Roselló-Mechó, M. Delgado-Pinar, A. Díez, and M. V. Andrés, "Measurement of Pockels' coefficients and demonstration of the anisotropy of the elasto-optic effect in optical fibers under axial strain," Opt. Lett. **41**(13), 2934 (2016).
6. M. Lindner, D. Bernard, F. Heilmeier, M. Jakobi, W. Volk, A. W. Koch, and J. Roths, "Transition from purely elastic to viscoelastic behavior of silica optical fibers at high temperatures characterized using regenerated Bragg gratings," Opt. Express **28**(5), 7323 (2020).
7. S. Spinner, "Elastic Moduli of Glasses at Elevated Temperatures by a Dynamic Method," J. Am. Ceram. Soc. **39**(3), 113–118 (1956).
8. Y. Shi, Y. Ma, and Y. Wang, "Magneto-elastic-optical coupling of Terfenol-D based optical fiber magnetic field sensors," Mater. Res. Express **6**(8), 086106 (2019).
9. S. DeWolf, F. K. Wyatt, M. A. Zumberge, and W. Hatfield, "Improved vertical optical fiber borehole strainmeter design for measuring Earth strain," Rev. Sci. Instrum. **86**(11), 114502 (2015).
10. Z. Zhang and F. Yu, "Quantitative analysis for the effect of the thermal physical property parameter of adhesive on the thermal performance of the quadrupolar fiber coil," Opt. Express **25**(24), 30513 (2017).
11. M. Fukuhara, A. Sanpei, and K. Shibuki, "Low Temperature-Elastic Moduli, Debye Temperature and Internal Dilational and Shear Frictions of Fused Quartz," J. Mater. Sci. **32**(5), 1207–1211 (1997).
12. F. El-Diasty, "Multiple-beam interferometric determination of Poisson's ratio and strain distribution profiles along the cross section of bent single-mode optical fibers," Appl. Opt. **39**(19), 3197 (2000).
13. K. O. Hill, B. S. Kawasaki, and D. C. Johnson, "cw Brillouin laser," Appl. Phys. Lett. **28**(10), 608–609 (1976).
14. K. S. Abedin, P. S. Westbrook, J. W. Nicholson, J. Porque, T. Kremp, and X. Liu, "Single-frequency Brillouin distributed feedback fiber laser," Opt. Lett. **37**(4), 605 (2012).
15. M. González-Herráez, K.-Y. Song, and L. Thévenaz, "Optically controlled slow and fast light in optical fibers using stimulated Brillouin scattering," Appl. Phys. Lett. **87**(8), 081113 (2005).
16. L. Thévenaz, "Slow and fast light in optical fibres," Nat. Photonics **2**(8), 474–481 (2008).
17. B. Vidal, M. A. Piqueras, and J. Martí, "Tunable and reconfigurable photonic microwave filter based on stimulated Brillouin scattering," Opt. Lett. **32**(1), 23 (2007).
18. J. Sancho, N. Primerov, S. Chin, Y. Antman, A. Zadok, S. Sales, and L. Thévenaz, "Tunable and reconfigurable multi-tap microwave photonic filter based on dynamic Brillouin gratings in fibers," Opt. Express **20**(6), 6157 (2012).
19. M. Santagiustina, S. Chin, N. Primerov, L. Ursini, and L. Thévenaz, "All-optical signal processing using dynamic Brillouin gratings," Sci. Rep. **3**(1), 1594 (2013).
20. M. Merklein, B. Stiller, K. Vu, S. J. Madden, and B. J. Eggleton, "A chip-integrated coherent photonic-phononic memory," Nat. Commun. **8**(1), 574 (2017).
21. T. Horiguchi, K. Shimizu, T. Kurashima, M. Tateda, and Y. Koyamada, "Development of a Distributed Sensing Technique Using Brillouin Scattering," J. Lightwave Technol. **13**(7), 1296–1302 (1995).

22. A. Denisov, M. A. Soto, and L. Thévenaz, "Going beyond 1000000 resolved points in a Brillouin distributed fiber sensor: theoretical analysis and experimental demonstration," Light: Sci. Appl. **5**(5), e16074 (2016).

23. Y. Tanaka and K. Ogusu, "Tensile-strain coefficient of resonance frequency of depolarized guided acoustic-wave Brillouin scattering," IEEE Photonics Technol. Lett. **11**(7), 865–867 (1999).

24. Y. Tanaka and K. Ogusu, "Temperature coefficient of sideband frequencies produced by depolarized guided acoustic-wave Brillouin scattering," IEEE Photonics Technol. Lett. **10**(12), 1769–1771 (1998).

25. N. Hayashi, K. Suzuki, S. Y. Set, and S. Yamashita, "Temperature coefficient of sideband frequency produced by polarized guided acoustic-wave Brillouin scattering in highly nonlinear fibers," Appl. Phys. Express **10**(9), 092501 (2017).

26. K. Shiraki and M. Ohashi, "Sound Velocity Measurement Based on Guided Acoustic-Wave Brillouin Scattering," IEEE Photonics Technol. Lett. **4**(10), 1177–1180 (1992).

27. Y. Antman, A. Clain, Y. London, and A. Zadok, "Optomechanical sensing of liquids outside standard fibers using forward stimulated Brillouin scattering," Optica **3**(5), 510 (2016).

28. D. M. Chow and L. Thévenaz, "Forward Brillouin scattering acoustic impedance sensor using thin polyimide-coated fiber," Opt. Lett. **43**(21), 5467 (2018).

29. D. M. Chow, Z. Yang, M. A. Soto, and L. Thévenaz, "Distributed forward Brillouin sensor based on local light phase recovery," Nat. Commun. **9**(1), 2990 (2018).

30. G. Bashan, H. H. Diamandi, Y. London, E. Preter, and A. Zadok, "Optomechanical time-domain reflectometry," Nat. Commun. **9**(1), 2991 (2018).

31. C. Pang, Z. Hua, D. Zhou, H. Zhang, L. Chen, X. Bao, and Y. Dong, "Opto-mechanical time-domain analysis based on coherent forward stimulated Brillouin scattering probing," Optica **7**(2), 176 (2020).

32. A. S. Biryukov, M. E. Sukharev, and E. M. Dianov, "Excitation of sound waves upon propagation of laser pulses in optical fibres," Quantum Electron. **32**(9), 765–775 (2002).

33. R. N. Thurston, "Elastic waves in rods and optical fibers," J. Sound Vib. **159**(3), 441–467 (1992).

34. R. M. Shelby, M. D. Levenson, and P. W. Bayer, "Guided acoustic-wave Brillouin scattering," Phys. Rev. B **31**(8), 5244–5252 (1985).

35. M. Abramowitz, I. A. Stegun, and D. Miller, "Handbook of Mathematical Functions With Formulas, Graphs and Mathematical Tables (National Bureau of Standards Applied Mathematics Series No. 55)," J. Appl. Mech. **32**(1), 239 (1965).

36. L. A. Sánchez, A. Díez, J. L. Cruz, and M. V. Andrés, "Efficient interrogation method of forward Brillouin scattering in optical fibers using a narrow bandwidth long-period grating," Opt. Lett. **45**(19), 5331 (2020).

37. L. Poveda-Wong, J. L. Cruz, M. Delgado-Pinar, X. Roselló-Mechó, A. Díez, and M. V. Andrés, "Fabrication of long period fiber gratings of subnanometric bandwidth," Opt. Lett. **42**(7), 1265 (2017).

38. S. P. Timoshenko and J. N. Goodier, *Theory of Elasticity*, McGraw-Hill, New York (1970).

39. D. York, N. M. Evensen, M. L. Martínez, and J. De Basabe Delgado, "Unified equations for the slope, intercept, and standard errors of the best straight line," Am. J. Phys. **72**(3), 367–375 (2004).